Simulation of radio signals from cosmic-ray cascades in air and ice as observed by in-ice Askaryan radio detectors.

Uzair Abdul Latif,[a] **Simon de Kockere,**[a,*] **Krijn de Vries,**[a] **Tim Huege,**[a,b] **Dieder Van den Broeck,**[a] **Stijn Buitink**[a] **and Nick van Eijndhoven**[a]

[a]*Vrije Universiteit Brussel (VUB),*
Pleinlaan 2, Brussels, Belgium

[b]*Karlsruhe Institute of Technology (KIT),*
PO Box 3640, 76021 Karlsruhe, Germany

E-mail: uzair.abdul.latif@vub.be, simon.de.kockere@vub.be

To detect the cosmic neutrino flux at the highest energies, Askaryan and radar radio detectors are being deployed in the polar regions. The in-ice Askaryan detectors use the radio detection technique to cover multi-gigaton detection volumes to probe neutrino interactions in the polar ice, whereas the in-ice radar technique aims to illuminate a large block of ice with a powerful radio transmitter to reflect radiowaves off particle cascades. Cosmic ray showers can serve as essential calibration sources for in-ice radio detectors. However, if not well understood, radio emissions from cosmic ray showers pose an essential background signal in the neutrino search. It follows that the neutrino signal is almost perfectly mimicked by cosmic-ray particle cascades moving from air to ice. We present a simulation framework to model the radio emissions from cosmic-ray showers by combining the in-air and in-ice radio emission frameworks to fully characterize the cosmic-ray radio signal as observed by the in-ice antennas.

ICRC2023
38th International Cosmic Ray Conference
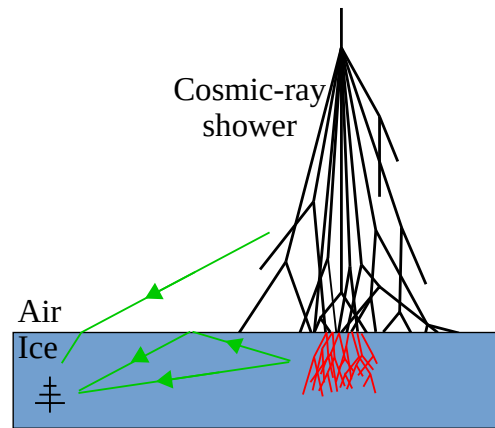The Astroparticle Physics Conference

---

*Speaker

1. Introduction

In-ice Askaryan radio detectors are being deployed in the polar regions to detect and measure coherent radio Cherenkov emission, known as Askaryan emission, resulting from the neutrino-induced in-ice particle cascades. Experiments like ARA, RNO-G, and ARIANNA have deployed radio antennas within the ice sheets of Greenland and Antarctica [1–3]. In addition, the in-ice radar technique is also being utilised by the Radar Echo Telescope (RET) to detect particle cascades from cosmic rays (RET-CR) and neutrinos (RET-N) [4]. This involves using a high-power radio transmitter to illuminate a large block of ice and then using receiver antennas to see the reflected radio pulse from particle cascades [5]. All of these experiments aim to measure the flux of high-energy cosmogenic and astrophysical neutrinos, surpassing the energies observed by IceCube ($> 10^{17}$ eV).

The radio signals produced by extensive air showers, particle cascades resulting from the interaction of ultra-high energy cosmic rays with the atmosphere play a crucial role as a background for Askaryan radio detectors. The radio signals emitted from cosmic ray-induced particle cascades share numerous similarities with radio signals from neutrino-induced in-ice particle cascades. In addition, high-energy cosmic rays also arrive with a considerably higher flux than high-energy neutrinos. Hence, cosmic rays offer an excellent calibration signal if their radio emissions can be understood and distinguished from those of neutrinos. In this work, we will combine the radio emissions from cosmic-ray signals from both in-air and in-ice cosmic-ray particle cascades as observed by in-ice

Figure 1: A schematic of a cosmic-ray shower penetrating an ice sheet. The green arrows indicate radio emissions going towards the in-ice antenna.

radio detectors. The latter occurs when high-energy cosmic ray cascades penetrate the high-altitude polar ice sheets. Figure 1 provides a diagram illustrating the development of the cosmic-ray particle cascade in air and then in ice after its penetration into a high-altitude ice sheet. The in-ice and in-air cosmic-ray radio emission frameworks have been discussed separately in other publications [6–8].

2. Cosmic-ray Cascade Simulations

This work will simulate cosmic-ray air shower in-air radio emissions with CoREAS (CORSIKA-based Radio Emission from Air Showers) [9]. CoREAS is a sub-module of the CORSIKA (COsmic Ray SImulations for KAscade) air shower simulation [10]. CoREAS uses the endpoint formalism to calculate the electric field emission from each shower particle (as simulated by CORSIKA) as the shower propagates and makes no assumptions regarding the emission mechanism. Since CORSIKA 7 only tracks radio emissions from particles in the air, we use GEANT4 for propagating cosmic-ray showers into ice. GEANT4 is a simulation code that tracks the passage of particles through any given medium [11].

Therefore, the in-air cosmic-ray shower framework is based on CoREAS, and the in-ice cosmic-ray shower framework is based on GEANT4. Both frameworks calculate radio emissions from the

shower particles through the endpoint formalism [6–8]. The implementation of the code for calculating radio emissions from particles in GEANT4 using endpoint formalism originates from the SLAC T-510 project [12]. The formalism works with the following expression to calculate the electric field emissions from individual particles [13]:

$$\vec{E}(\vec{x}, t) = \frac{q}{c} \left[\frac{\hat{r} \times [(\hat{r} - n\vec{\beta}) \times \dot{\vec{\beta}}]}{(1 - n\vec{\beta}.\hat{r})^3 \, R} \right]_{\text{ret}} \tag{1}$$

The original CoREAS code has only been designed to work in the air using straight-line ray propagation, and Eq. 1 has only been used up till now with straight-line ray propagation parameters. In reality, air and ice have density-dependent exponential refractive index profiles that cause radiowave rays to bend as they propagate toward an observer.

In the upcoming sections, it will be discussed how Eq. 1 can be adjusted such that it incorporates the full ray bending effect in air and ice. We will also discuss the addition of several other important features, such as the calculation of Fresnel coefficients and of the ray focusing factor and the simulation of transition radiation. These features are required to fully 'complete' the cosmic-ray shower simulation.

3. Refractive Index Profiles of Air and Ice

The ice refractive index profile of ice can be parameterized in the form of:

$$n(z) = A + B \exp(-Cz) \tag{2}$$

The refractive index profile of a specific medium can be uniquely determined by the values of its parameters: A, B, and C. A represents the asymptotic value of the refractive index. When considering polar ice, z corresponds to the depth beneath the surface of the ice.

The parameters will be defined as $A = 1.78$, $B = -0.43$ and $C = -0.0132$ m^{-1} which are also used by the ARA and RICE experiments located at South Pole [14].

The air density model for particle cascade simulations in CORSIKA follows a 5-layer structure, with each layer exhibiting an exponential profile. The atmosphere refractive index profiles are extracted from the GDAS-tool, which provides tabulated refractivity profiles considering density, humidity, and location-specific factors [8].

4. Interpolation of Raytracing Parameters

Raytracing is the exercise of tracing the path of radiowaves as they propagate through a given medium (i.e. air or ice). To perform raytracing, we use analytic expressions that depend on smooth exponential refractive index profiles of a given medium [8, 15, 16]. In this work, raytracing is performed using a 'flat Earth' approximation, which is valid for cosmic-ray cascades with zenith angles up to $\sim 65°$.

Propagating rays from each shower particle at each step to each antenna could take weeks or months, depending on the shower energy and the number of in-ice antennas. Therefore, directly using the analytic raytracing functions is not feasible, and we have to move towards interpolation [8]. Interpolation of ray parameters from pre-made tables makes the raytracing process considerably faster. The percentage error for the interpolated results is around $O(10^{-5}\% - 10^{-6}\%)$, which is sufficiently accurate for our purpose [8].

5. Adding Raytracing to the In-air and In-ice Emission Frameworks

Incorporating raytracing parameters in the CoREAS in-air radio emission framework and the GEANT4-based in-ice radio emission framework is relatively straightforward. In order to perform raytracing, Eq. 1 gets modified in the following way:

1. the angle of the $\vec{\beta} . \hat{r}$ dot product is replaced with the launch angle obtained from raytracing.

2. R gets replaced with the value of the geometrical path length of the ray in air and ice.

3. the value of n is taken to be the refractive index value at the emission point.

Modifications 1 and 3 have been discussed in detail in another work [17]. It has been shown that these modifications align with physics and allow for the 'correct' integration of raytracing in both the in-air and in-ice frameworks.

To account for the effect of ray bending, the final received electric field vector has to be rotated in the plane of incidence of the ray. This is to account for the difference in the launch and receive angles of the 'bent' ray. The magnitude of the rotation angle is given by the difference between the launch and receive angles of the ray.

6. Fresnel Coefficients

To correctly calculate the final electric field amplitude observed by the in-ice antenna, it is important to calculate Fresnel coefficients for the electric field ray paths in two cases. In the first case, the in-air ray enters the ice surface and refracts towards the antenna, and here we need to calculate the transmission coefficient to calculate the final electric field amplitude of the transmitted pulse. In the second case, the second in-ice pulse gets reflected from the ice surface towards the radio antenna, and here we need to calculate the reflection coefficient to calculate the final electric field amplitude of the reflected pulse. In both cases, the coefficients are essentially scaling factors for the final observed electric field at the in-ice antenna and are a function of the incident ray angles and refractive index values of air and ice at the air-ice boundary. The Fresnel coefficients for the S and P electric field polarizations can be calculated using the following expressions:

$$r_S = \frac{n_1 \cos(\theta_i) - n_2 \sqrt{1 - \left(\frac{n_1}{n_2} \sin(\theta_i)\right)^2}}{n_1 \cos(\theta_i) + n_2 \sqrt{1 - \left(\frac{n_1}{n_2} \sin(\theta_i)\right)^2}} \quad (3) \qquad t_S = 1 + r_S \quad (5)$$

$$r_P = -\frac{n_1 \sqrt{1 - \left(\frac{n_1}{n_2} \sin(\theta_i)\right)^2} - n_2 \cos(\theta_i)}{n_1 \sqrt{1 - \left(\frac{n_1}{n_2} \sin(\theta_i)\right)^2} + n_2 \cos(\theta_i)} \quad (4) \qquad t_P = (1 + r_P)\frac{n_1}{n_2} \quad (6)$$

Here θ_i is the angle of incidence on the ice surface, and n_1 and n_2 are the refractive index values of the first and the second medium at the boundary. The ordering of the two media (i.e. air and ice) can differ depending on whether a ray is being reflected down from the ice surface or transmitted through from above the ice surface. r_S and r_P are reflection coefficient values, and t_S and t_P are transmission coefficient values for the S and P polarisations of the electric field, respectively. It is

also important to note that Eqns. 3, 4, 5 and 6 only hold for the approximation $\mu_1 \approx \mu_2 \approx \mu_0$ which can be made for the case of the air-ice boundary. It should also be noted that for θ_i greater than the critical angle, the phase shifts on total reflection are deduced from complex values of the reflection coefficients. The calculation of these complex phase shifts is non-trivial and has been ignored for now.

7. Focusing Factor & Transition Radiation

The focusing factor (F) is an additional factor that must be considered while calculating the final observed electric field amplitude. In a media with an exponential density profile, rays converge near the 'shadow zone' boundary. Although raytracing is an exercise carried out for infinitesimal points in the media, in reality, neither our antennas nor emitting particles are infinitesimal points. Therefore, whenever an antenna receives a high density of rays from an emitter, an amplification in the electric field amplitude is expected. The mathematical expression for calculating F has been exported from NuRadioMC [18]. We also limit F to a maximum value of 2, as in NuRadioMC. It is important to note that for the in-ice case, we consider both the possible direct and indirect ray paths between two points within the ice sheet.

As shown in [13], the endpoint formalism naturally includes the emission of transition radiation when the calculations of the emission in the first medium and the emission in the second medium are done separately. The in-air simulation by CoREAS will generate the sudden death emission, while the continuation of the simulation by the GEANT4 module will lead to the sudden appearance emission. The combination of both gives the transition radiation.

8. Results

All cosmic-ray showers that will be discussed in this section were simulated with some specific CoREAS settings. THINNING was set to be ON in order to have reasonable simulation times. The thinning threshold was set at 1×10^{-6} with the maximum weight being 100. The energy of the primary particle was set to be 1×10^{17} eV, and the zenith and azimuth angles were set to be at $0°$ (i.e. the direction of the shower was vertically downwards). The altitude of the ice sheet was fixed to be 2.835 km. The selected high-energy and low-energy particle interaction models were QGSJETII-04 and UrQMD, respectively. Finally, all the simulations were performed for a star-shaped antenna grid which included 120 antennas and was located at an ice depth of 150 m. The hit point of the shower core was set to be the centre of the star grid on the ice surface.

The electric field waveforms from the simulated cosmic ray shower are shown in Fig. 2 for the electric field's North and West and Vertical components. The positions of the four antennas from where the electric fields were obtained have been indicated by a schematic at the top of Fig. 2. Antennae 0 and 3 are closer to the outer edge of the antenna star grid and hence are closer to the emission point of the in-ice Cherenkov cone. Whereas antennae 1 and 2 are closer to the centre of the star grid and the shower core and hence closer to the in-air Cherenkov emission point. Therefore, the electric field waveforms in Fig. 2 show that in-air emissions are stronger than in-ice emissions in antennae 1 and 2, and for antennae 0 and 3, it is the opposite. It can also be inferred from the waveforms in Fig. 2 that as we move further outward from the centre of the star grid, the difference in time arrival between in-air and in-ice emissions also increases. One final thing to note is the
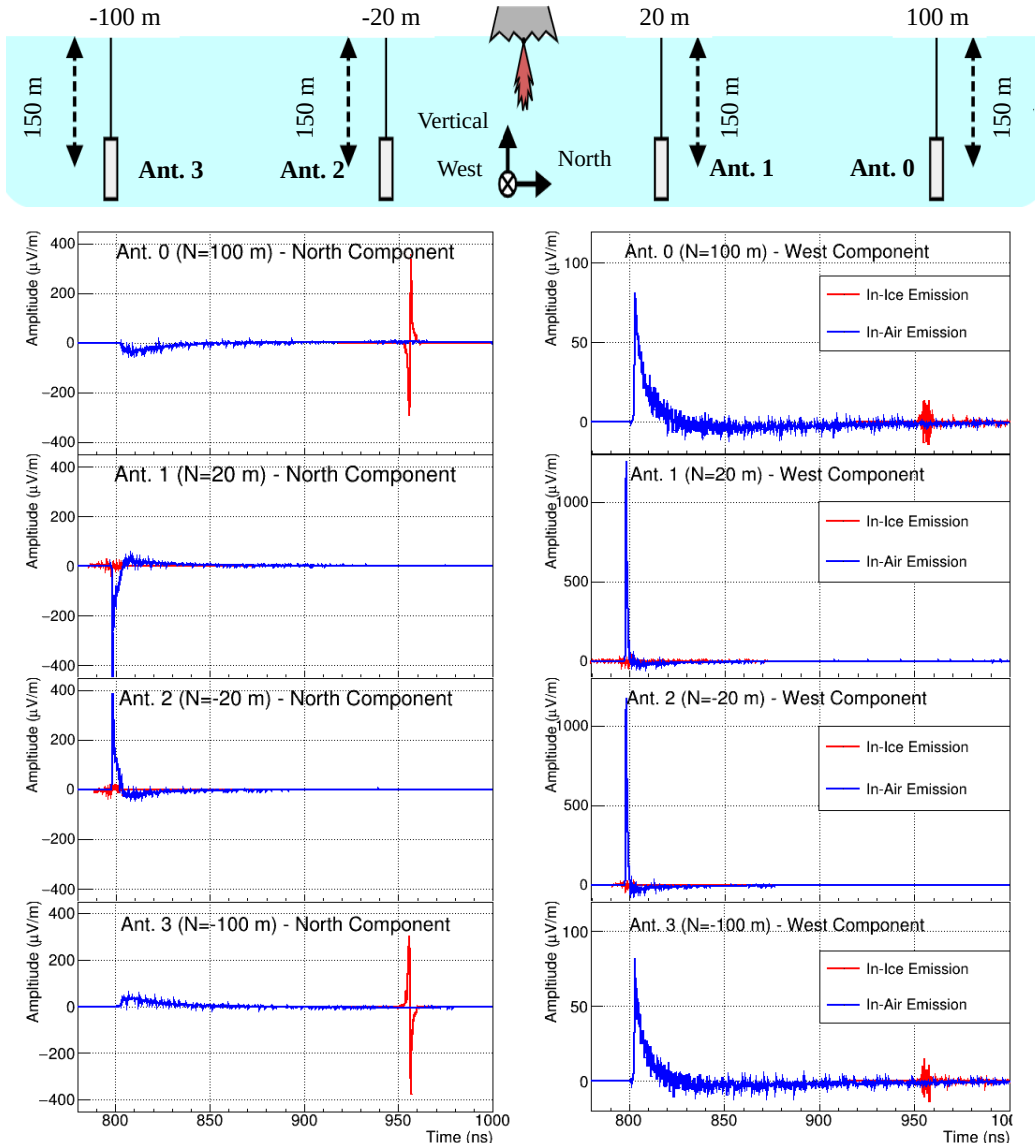
Figure 2: The observed electric field pulses at 4 antenna locations. The schematic at the top indicates the selected antennas and their positions around the shower core. The two columns of waveforms show the simulated electric field pulses for in-air (blue) and in-ice (red) emissions for North (left) and West (right) electric field components, respectively. The distance in the title brackets indicates the distance of the antenna to the shower core along the North axis.

polarity flip in the North electric field component when we move across the shower core from antenna 1 to 2 along the North axis. We only observe the in-air energy fluence shower asymmetry along the West axis, and therefore along the North axis, the Askaryan emission dominates, which leads to the polarity flip. Therefore, as expected in the case of the West axis, the in-air geomagnetic emission dominates; hence, no polarity flip is observed for the West electric field component when we move across the shower core.

The cosmic-ray shower radio footprint, as observed 150 m ice depth, is shown in Figs. 3. The simulated electric field pulses at each antenna location in the star grid were used to calculate the
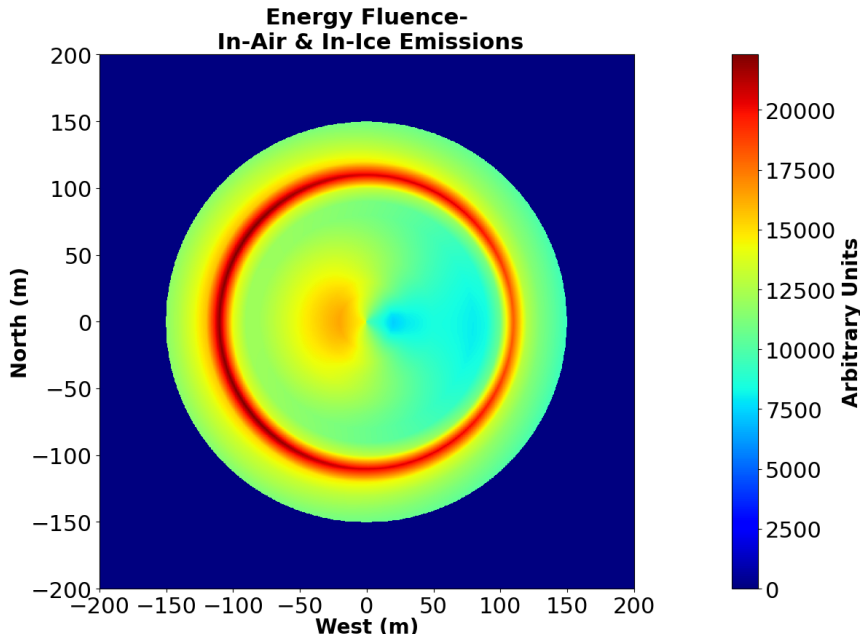
Figure 3: The shower radio footprint for a vertical cosmic-ray shower observed at -150 m depth in the ice. Antennas were placed in a star-shaped configuration, and the total energy fluence received by each antenna was recorded. 2-D interpolation was then used to construct the footprint [19]. The colour scale on the z-axis shows the energy fluence observed at each point.

total energy fluence. The entire footprint was then generated using 2-D interpolation between the antenna positions. First, we notice the anisotropy in received power across the footprint caused by the interference between in-air Askaryan and in-air geomagnetic emission mechanisms [20]. The Cherenkov ring caused by the in-ice emission can also be seen closer to the outer edge of the footprint. A slight asymmetry on the Cherenkov ring indicates the interference between in-air geomagnetic emissions and in-ice Askaryan emissions. As the in-ice shower evolves, the in-ice Cherenkov angle increases with the rapidly increasing ice density and refractive index. This causes the in-ice Askaryan emission to be spread over a circular band around the outer edge of the antenna grid, and hence the overall energy fluence also remains pretty strong till the outer edges of the band.

9. Conclusion

We now have a fully functioning cosmic-ray cascade radio emission simulation that incorporates all the important features like exponential refractive index and density profiles of air and ice, Fresnel coefficients, focusing factor, and transition radiation. The results of the simulation are consistent with the expected physics. The following steps will further investigate the results at varying shower geometries and integrate this simulation framework into CORSIKA 8 [21].

10. Acknowledgements

References

[1] ARA collaboration, *Constraints on the diffuse flux of ultrahigh energy neutrinos from four years of askaryan radio array data in two stations*, *Phys. Rev. D* **102** (2020) 043021.

[2] J.A. Aguilar *et al*, *Design and sensitivity of the radio neutrino observatory in greenland (RNO-g)*, *Journal of Instrumentation* **16** (2021) P03025.

[3] A. Anker *et al*, *Probing the angular and polarization reconstruction of the ARIANNA detector at the south pole*, *Journal of Instrumentation* **15** (2020) P09039.

[4] S .Prohira *et al*, *The Radar Echo Telescope for Cosmic Rays: Pathfinder experiment for a next-generation neutrino observatory*, *Phys. Rev. D* **104** (2021) 102006 [2104.00459].

[5] S .Prohira *et al*, *Observation of Radar Echoes from High-Energy Particle Cascades*, *Phys. Rev. L* **124** (2020) 091101 [1910.12830].

[6] S. De Kockere *et al*, *Simulation of the propagation of cosmic ray air showers in ice*, vol. ARENA2022, p. 015, 2023, DOI.

[7] S. De Kockere *et al*, *Simulation of in-ice cosmic ray air shower induced particle cascades*, *Phys. Rev. D* **106** (2022) 043023.

[8] U. A. Latif *et al*, *Propagating air shower radio signals to in-ice antennas*, vol. 424, p. 016, June, 2023, DOI.

[9] T. Huege *et al*, *Simulating radio emission from air showers with CoREAS*, *AIP Conf. Proc.* **1535** (2013) 128 [1301.2132].

[10] D. Heck *et al*, *CORSIKA: A Monte Carlo code to simulate extensive air showers*, *FZKA* **6019** (1998) .

[11] J. Allison *et al*, *Recent developments in geant4*, *Nuclear Instruments and Methods in Physics Research Section A: Accelerators, Spectrometers, Detectors and Associated Equipment* **835** (2016) 186.

[12] K. Belov *et al*, *Accelerator Measurements of Magnetically Induced Radio Emission from Particle Cascades with Applications to Cosmic-Ray Air Showers*, *Phys. Rev. L* **116** (2016) 141103 [1507.07296].

[13] C. W. James *et al*, *General description of electromagnetic radiation processes based on instantaneous charge acceleration in "endpoints"*, *Phys. Rev. E* **84** (2011) 056602.

[14] J. Kelley *et al*, *Observation of two deep, distant (1.4, 4)km impulsive RF transmitters by the Askaryan Radio Array (ARA).*, *PoS* **ICRC2017** (2018) 1030.

[15] U.A. Latif, *Towards measurement of UHECR with the ARA experiment*, Ph.D. thesis, University of Kansas, 2020.

[16] U. Latif, "Iceraytracing." https://github.com/uzairlatif90/IceRayTracing, 2023.

[17] D. Van den Broeck *et al*, *Radio propagation in non-uniform media*, vol. ARENA2022, p. 020, 2023, DOI.

[18] C. Glaser *et al*, *NuRadioMC: simulating the radio emission of neutrinos from interaction to detector*, *European Physical Journal C* **80** (2020) 77.

[19] A. Corstanje *et al*, *A high-precision interpolation method for pulsed radio signals from cosmic-ray air showers*, *arXiv e-prints* (2023) arXiv:2306.13514 [2306.13514].

[20] K. de Vries *et al*, *The lateral distribution function of coherent radio emission from extensive air showers: Determining the chemical composition of cosmic rays*, *Astroparticle Physics* **34** (2010) 267.

[21] J. Ammerman-Yebra *et al*, *Simulations of cross media showers with CORSIKA 8*, *PoS* **ICRC2023** (2023) 442.